A ∼300 pc-sized core of Milky Way dark matter halo constrained from the OGLE micro-lensing sky map

Shurui Lin,[1, *] Wentao Luo,[1, †] Yi-Fu Cai,[1, ‡] Qi Guo,[1] Leyao Wei,[2]

Bo Wang,[1] Qinxun Li,[1] Canpo Su,[1] and Alexander Rodriguez[3]

[1] *CAS Key Laboratory for Researches in Galaxies and Cosmology/Department of Astronomy,*
School of Astronomy and Space Science, University of Science and Technology of China, Hefei, Anhui 230026, China
[2] *School of Physics and Astronomy, Sun Yat-sen University, 2 Daxue Road, Zhuhai 519082, China*
[3] *Department of Astronomy, University of Michigan, 1085 S. University, Ann Arbor, MI 48109*

We report the detection of a 282^{+34}_{-31} pc-sized core in the center of Milky Way dark matter halo at 68% confidence level by using the micro-lensing event rate sky map data from the Optical Gravitational Lensing Experiment (OGLE) survey. We apply the spacial information of the micro-lensing sky map and model it with the detailed Milky Way dark matter halo Core/Cusp profile, and the fraction of dark matter in the form of Mini Dark Matter Structure (MDMS, $f_{\mathrm{MDMS}} = \Omega_{\mathrm{MDMS}}/\Omega_{\mathrm{DM}}$), e.g. primordial black hole, earth-mass subhalos, floating planets and so on. We find that this sky map can constrain both f_{MDMS} and the core size simultaneously without strong degeneracy while fully considering mass function of Milky Way stellar components from both the bulge and disk.

Introduction – The concordance cosmology is such a successful model that it fits most of the observations with only half a dozen parameters, e.g. Cosmic Microwave Background (CMB) [1], Supernova Ia (SNIa) [2], time delay projects based on strongly lensed Active Galactic Nuclei (AGNs) [3], and weak lensing statistics [4]. However, despite all these successes, tensions emerge among different cosmological probes, e.g. the recent Hubble tension between the Planck observation and SNIa [5], the "lensing is low" issue on cosmological parameters between weak-lensing measurements and CMB [6].

At small scales, there exist a series of "crises" as well, including the missing satellite problem (MSP), too big to fail (TBTF), as well as the core-cusp problem (CCP) [7]. Especially, the core-cusp issue, where the inferred dark matter core structure from nearby dwarf galaxies contradicts the Navarro-Frenk-White (NFW) profile, a cuspy profile from pure cold dark matter simulations [8], leads to the extensive study on the formation mechanism of the core structure either from an exotic self-interacting dark matter (SIDM) model [9, 10], or an astrophysical model from baryonic feedback and merging, dynamical friction, e.t.c. [see review papers of [11, 12]]. It was suggested in Debattistal et al 1998[13] that the dark matter halo in the Milky Way could also hold a core structure via simulations. Moreover, the enigmatic Gould Belt can be created by a "dark matter core" colliding with the gas disk of the Milky Way [14, 15]. However, so far there is no conclusive observational evidence to either confirm or reject the aforementioned core structure of Milky Way. This is largely due to the fact that dark matter itself can not be directly observed and the rotation curve of the Milky Way is not as informative as nearby dwarf galaxies [15, 16]. Zoom-in hydro simulations [17, 18] can provide information on the core formation of Milky Way halos via a baryonic feedback mechanism, yet it lacks concrete observational evidence due to the data quality of the Milky Way rotation curve. New probes are then necessary for mapping the dark side of the Milky Way and comparing to simulations, which will boost our understanding of the core formation of the Milky Way halo and the like.

The method we develop here is based on the assumption that a fraction of dark matter is in form of primordial black holes[19–21], dark matter halos with hundreds of earth masses [22], or to a very recent work [23]: the so-called dark matter minihalos with extremely high internal density of $10^{12} M_\odot/\mathrm{pc}^3$. We generalize it as mini dark matter structures (MDMS) that follow the density profile of the Milky Way dark matter halo and can induce the micro-lensing event when intervening in the line between the background star and the observer. Fig.1 presents the patterns of the micro-lensing event rate map between the cuspy NFW profile (left panel) and the cored density profile (middle panel). The right panel is the event rate sky map of OGLE's newest data release [24]. By fitting the OGLE sky map, we can constrain the dark matter density profile.

Here, we serendipitously found that the spatial distribution of micro-lensing event rate sky map targeting the Galactic center from Optical Gravitational Lensing Experiment (OGLE) [25] can put strong constraints simultaneously on both Mini Dark Matter Structures (MDMS) fraction, and the core size of the central part of Milky Way dark matter halo. The inferred size of the dark core is 282^{+34}_{-31}pc at 68% confidence level. Further, this result can put constraints on both dark matter models beyond cold dark matter (CDM) or the baryonic physics of the Milky Way [26]. Either way, this discovery opens another window to peek at the mystery of the core-sups problem.

Micro-lensing model – Our model extends the micro-lensing geometry and notations in Niikura et al. 2019 [27] by fully employing the spacial information. We take the x-direction to be along the line connecting the Galactic center and the Earth (the observer's position), with the assumption that the Earth is located
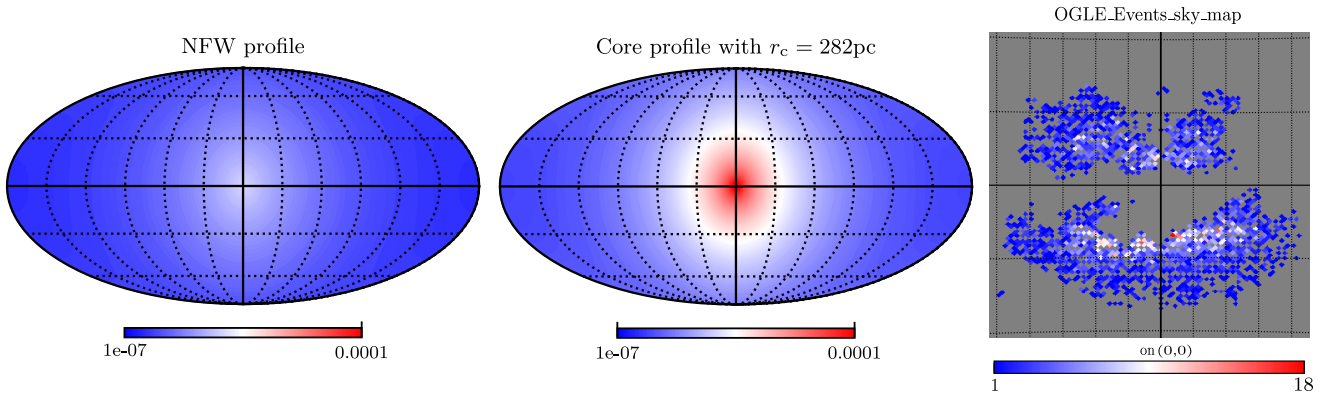
FIG. 1. The sky-maps are plotted in Mollweide projection.
Left panel: Micro-lensing event rate given an NFW density profile;
Middle panel: 282pc core size event rate;
Right panel: The sky map of 5790 OGLE micro-lensing events. The difference between graticules are 2 degrees in longitude and 4.5 degrees in latitude
As we are unable to reach all the detailed data of micro-lensing events used to build the catalog, we can not plot an event-rate sky map [Readers can find it in Fig.24 of [25]].

at $(x, y, z) = (8\text{kpc}, 0, 0)$. The y-direction is the rotating direction of the Earth in the Galactic disk plane together with the z-direction being perpendicular to the plane.

In this paper, we denote the mass of the lens as M, while the source-observer, lens-observer, and source-lens distance as d_s, d_l and $d_{ls} = d_s - d_l$. In our coordinate system, a lens at d_l will be located at: $x = 8\text{kpc} - d_l \cos l \cos b$, $y = d_l \cos b \sin l$, $z = d_l \sin b$. As the OGLE survey mainly focuses on the source near the Galactic center, we assume $d_s = 8$ kpc for all the sources as has been done in Niikura et al. 2019 [27]. With the above notation, the Einstein radius R_E for a given mass M can be expressed as:

$$R_{\mathrm{E}} = \sqrt{\frac{4GM}{c^2} \frac{d_{\mathrm{l}} d_{\mathrm{ls}}}{d_{\mathrm{s}}}} \qquad (1)$$

For simplicity, we consider that all the lenses have an identical mass of M for MDMS, but stellar mass function (see the following section) for bulge and disk contribution. Both of them follow the Maxwell-Boltzmann velocity distribution (we also test a different velocity distribution to examine if the core size varies accordingly in the supplemental appendix). To be specific, as we are only interested in the relative velocity between lenses and source that is perpendicular to the x direction, the velocity distribution has the following form:

$$f(\mathbf{v}_{\perp}) = \frac{1}{2\pi\sigma_y\sigma_z} \exp\left[\frac{(v_{\perp}\cos\theta - \bar{v}_y)^2}{\sigma_y^2} + \frac{(v_{\perp}\sin\theta - \bar{v}_z)^2}{\sigma_z^2}\right]$$
$$(2)$$

where θ represents the direction of $\mathbf{v}_{\perp}$, σ_y, σ_z are the velocity dispersion of lens in the y and z directions and $\bar{v}_y$, $\bar{v}_z$ are the mean velocity along y and z directions.

With the above assumptions, the micro-lensing event rate for timescale t_E along a certain direction is then:

$$\frac{\mathrm{d}\Gamma_{\mathrm{d}}}{\mathrm{d}t_{\mathrm{E}}} = \pi \int \mathrm{d}(\ln M) \frac{\mathrm{d}n_{\mathrm{lens}}(M)}{\mathrm{d}\ln M} \int_0^{d_{\mathrm{s}}} \mathrm{d}d_{\mathrm{l}} \frac{\rho_{\mathrm{lens}}(d_{\mathrm{l}})}{M}$$
$$\int_{-\pi/2}^{\pi/2} \mathrm{d}\theta v_{\perp}^4 f_{\mathrm{lens}}(v_{\perp}, \theta) \qquad (3)$$

where t_E is given by $t_E = (2R_E\cos\theta)/(v_{\perp})$. And $\rho_{\mathrm{lens}}(d_l)$ is the density profile for lenses' distribution along the line of sight at the distance of d_l, whose specific expression depends on its kind, i.e. dark matter, bulge stellar and disk stellar. $\frac{\mathrm{d}n_{\mathrm{lens}}(M)}{\mathrm{d}\ln M}$ is the mass function of lens. We assume a delta mass function for MDMS and will discuss the detailed mass function of stellar components in the following sections.

As the density profile is only considered in the integration along the line of sight, the angular distribution of the density profile is encoded inside the event rate distribution.

For cusp-like dark matter halo, we adopt the NFW density profile:

$$\rho_{\mathrm{NFW}}(r) = \frac{\rho_{\mathrm{c}}}{(r/r_{\mathrm{s}})(1 + r/r_{\mathrm{s}})^2} \qquad (4)$$

where r is the distance to the Galactic center, $\rho_{\mathrm{c}} = 4.88 \times 10^6 M_{\odot}/\text{kpc}^3$ and $r_{\mathrm{s}} = 21.5\text{kpc}$. For a core-liked halo, we choose the Berkurt density profile [28]:

$$\rho_{\mathrm{Bk}}(r) = \frac{\rho_{\mathrm{b}}}{(1 + r/r_{\mathrm{b}})(1 + (r/r_{\mathrm{b}})^2)} \qquad (5)$$

where r_b stands for the core size and ρ_b is determined by the halo mass. Here we assume the Milky Way halo mass to be of $10^{12} M_{\odot}$ [29]. The density profile and velocity

Lens' kind	Density profile $\rho[M_\odot/\mathrm{pc}^3]$	Velocity profile (μ,σ) [km/s]
Bulge	$1.04 \times 10^6 (\frac{s}{0.482\mathrm{pc}})^{-1.85}, \ (s < 938\mathrm{pc})$	$f_y : \{-220(1-\alpha), 100\sqrt{1+\alpha^2}\}$
	$3.53 \ K_0(\frac{s}{667\mathrm{pc}}), \ (s \geq 938\mathrm{pc})$	$f_z : \{0, 100\sqrt{1+\alpha^2}\}$
Disk	$0.06 \times \exp[-\{\frac{R-8000}{3500} + \frac{z}{325}\}]$	$f_y : \{220\alpha, \sqrt{(\kappa\delta+30)^2 + (100\alpha)^2}\}$
		$f_z : \{0, \sqrt{(\lambda\delta+30)^2 + (100\alpha)^2}\}$
MDMS	Cusp: $4.88 \times 10^{-3} \frac{1}{(r/r_\mathrm{s})(1+r/r_\mathrm{s})^2}$	$f_y : \{-220(1-\alpha), \sqrt{220^2 + (100\alpha)^2}\}$
	Core: $\frac{\rho_\mathrm{b}}{(1+r/r_\mathrm{b})(1+(r/r_\mathrm{b})^2)}$	$f_z : \{0, \sqrt{220^2 + (100\alpha)^2}\}$

TABLE I. Density profile and velocity profile for each kind of lens, where $\alpha = d_\mathrm{l}/d_\mathrm{s}$, $\kappa = 5.625 \times 10^{-3}$km/s/pc, $\lambda = 3.75 \times 10^{-3}$km/s/pc, $\delta = (8000-x)$pc, $K_0(x)$ is modified Bessel function and R$=(x^2+y^2)^{\frac{1}{2}}$, $s^4 = R^4 + (z/0.61)^4$, $r^2 = x^2+y^2+z^2$

profile we use for each component of lens are shown in Table.1 [27].

Mass function of Stellar Components – In order to estimate the event rate of stellar components in bulge and disk, we need to get the mass function of each kind. For this purpose, we assume the Kroupa broken power-law initial mass function (IMF)[30].

$$\frac{\mathrm{d}n_\mathrm{s}(M)}{\mathrm{d}\ln M} = \begin{cases} A_\mathrm{MS}\left(\frac{M}{M_\mathrm{break}}\right)^{1-\alpha_\mathrm{MS1}} & (M \leq M_\mathrm{break}) \\ A_\mathrm{MS}\left(\frac{M}{M_\mathrm{break}}\right)^{1-\alpha_\mathrm{MS2}} & (M \geq M_\mathrm{break}) \end{cases} \quad (6)$$

Following previous work [27], we assume all stars within the initial mass range $[1 \leq M_\mathrm{break}/M_\odot \leq 8]$ evolves into White Dwarfs following initial-final mass relation of :$M_\mathrm{WD} = 0.339 + 0.129 M_\mathrm{init}$ and stars with $[8 \leq M_\mathrm{break}/M_\odot \leq 20]$ into neutron stars following a Gaussian distribution with mean value $M_\mathrm{final} = 1.39 M_\odot$ and width $\sigma = 0.12 M_\odot$.

We choose the newer data from Mróz et al. 2020 [25] instead of the previous version based on Mróz et al. 2017 [31] which only contains 9 fields. Here, we set $\alpha_\mathrm{MS2} = 2$, $M_\mathrm{break} = 0.5 M_\odot$, and leave α_MS1 as free parameter to be sampled by MCMC. We choose $\alpha_\mathrm{MS1} = 1.1$ as the fiducial value, which is consistent with the result from Sagittarius Window Eclipsing Extrasolar Planet Search (SWEEPS)[32].

Fitting to data – Before proceeding with MCMC, we need to subtract the contribution of bulge and disk components in event rates sky map. That is:

$$\Gamma_\mathrm{fixed,k} = \Gamma_\mathrm{OGLE,k} - \Gamma_\mathrm{bulge,k} - \Gamma_\mathrm{disk,k} \quad (7)$$

where k is the index of fields in the OGLE survey. Afterwards, we neglect all the fields with negative values and use the remaining 55 fields, where we choose to fit two variables: the fraction of MDMS (f_MDMS) and the size of the core ($\log_{10} r_\mathrm{b}$) by fitting the theoretical event rate Γ_Core to the event rate at the directions of 55 fields. For simplicity, we assume a log-normal likelihood function:

$$\ln(p) = \sum_{\mathrm{k}=1}^{55} -\frac{(\ln(\Gamma_\mathrm{Core,k}) - \ln(\Gamma_\mathrm{fixed,k}))^2}{2\sigma_\mathrm{k}^2} + \ln(\sigma_\mathrm{k}) \quad (8)$$

σ_k in the above formula is given by $\sigma_\mathrm{k}^2 = \ln(1 + \sigma_\mathrm{OGLE,k}^2/\Gamma_\mathrm{fixed,k}^2)$ in which $\sigma_\mathrm{OGLE,k}$ is the error of event rate from the OGLE data.

Based on the likelihood function, we use the python package EMCEE[33] to run MCMC with 20 walkers and 3500 steps each after burn-in processes of 500 steps. The posteriors of the two parameters are therefore sampled from the chains.

Result We perform a test by calculating the Bayesian factor for both the cuspy profile (NFW formula) and the core profile (Burkert formula) with the nested sampling Monte Carlo algorithm MLFriends [34][35] using the UltraNest package [36] . For all the lens mass we tested, the ratios between Bayesian factors of the Burkert profile and NFW profile are larger than 10^3. This illustrates that the Burkert density profile is much more probable than the NFW profile.

The major results are shown in Fig.2, the top left panel presents the posterior distribution of core size $(\log_{10}(r_\mathrm{b}/\mathrm{pc}))$ and the fraction of MDMS (f_{MDMS}) assuming the lens mass of $\sim 10^{-2} M_\odot$. The latter varies significantly as a function of lens mass due to the OGLE survey cadence (the bottom panel of Fig.2). Nonetheless, the core size remains consistent with the fiducial value that the lens is set to be one solar mass (red solid line with one sigma pink shaded region in the top right panel of Fig.2). The effective range is between $10^{-3} M_\odot$ and $10^0 M_\odot$, where the constraint is the most effective based on OGLE survey data.

Astonishingly, for lens' mass around $10^{-3} M_\odot$, f_MDMS is about 10^{-3}. That means, to the maximum, $10^9 M_\odot$ dark matter is in the form of MDMS, which is a much stronger constraint than previous result[27]. The dependence of f_MDMS on lens mass is due to the cadence of OGLE survey which is in $[0.1\mathrm{days}, 300\mathrm{days}]$. As a result, when lens' mass is too large($> 1 M_\odot$) or too small($< 10^{-3} M_\odot$), the constraint on f_MDMS is approaching to 1. The bottom panel of Fig.2 clearly shows the dependence of f_MDMS on lens stellar mass, which is purely introduced by the OGLE survey cadence.

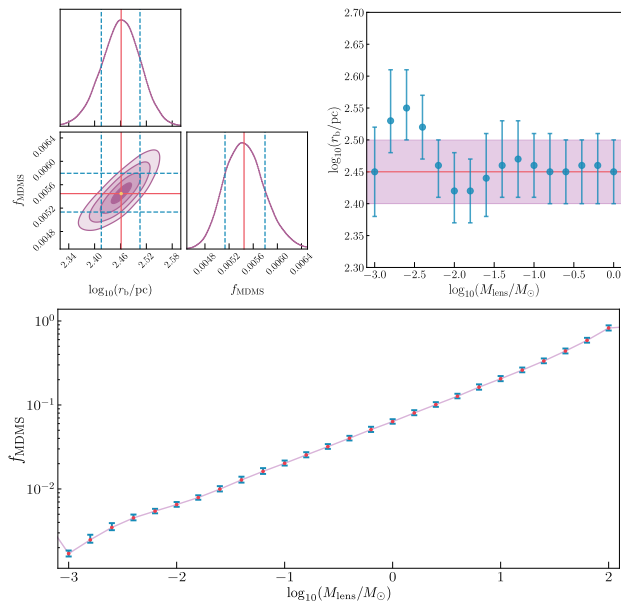*Concluding remarks* – Back in the 1990s, Navarro, Frenk, and White [37] have already noticed the discrep-

FIG. 2. *Top left:* The corner plot of the two parameters f_{MDMS} and core size r_b with lens mass of $10^{-2.2} M_\odot$. The red solid lines are the median value of the posterior distribution and the blue dashed lines denote the 68% confidence interval. The yellow point is the median value of MCMC sampled posterior and different contours in the corner plot denote the different σ levels.
Top right: The core size as a function of lenses' mass. The red solid line is the median value from the left panel for r_b with one sigma range as the purple belt. The different core sizes sampled from different lens mass is shown as the data points with error bars. The value remains almost unchanged within one sigma level.
Bottom: Fraction of MDMS f_{MDMS} from MCMC as function of lenses' mass. The red points are the median with blue errorbars showing the one sigma range for each mass value. The purple solid line connects the median values.

ancy between the CDM simulated cuspy halo and the core structure of dwarf galaxies. They attribute the formation of the core to the perturbations in the inner region caused by the "vigorous" star formation process. The high-resolution FIRE simulation [26] explores the galaxy formation, and at the same time, the Milky Way halo exhibits a core structure formed in the central region due to stellar feedback. In Chan et al 2015, [17] they generate a suite of simulations based on the same code of FIRE, focusing on the core size of galaxies with a wide range of stellar mass and feedback. Their results present much larger core sizes than ours ranging from 1.2kpc to 2.0kpc for Milky Way dark matter halo. Our results show a much smaller core size that caused by the baryonic feedback in those simulations.

On the other hand, phenomenological models beyond CDM provide another means to interpret the core structure formation, ranging from a solitonic core of ultra-light dark matter (ULDM) [38], or fuzzy dark matter (FDM) [39], to self-interacting dark matter (SIDM) [40] as well as weakly interacting massive particles (WIMP) [41]. However, the core size of the dark matter halo behaves differently in the stellar feedback scenario from one of those models, specifically the SIDM model[42]. The former shows the core size peaks around $\log_{10}(\mathrm{M}_*/\mathrm{M}_\odot) \sim 10.0$ while the latter illustrates a monotonic increase as a function of halo mass. In general, different dark matter particle models can potentially be tested by astrophysical observations, such as modulated Einstein rings from multiple image systems of strong-lensing events [43]. We present a novel method to probe the dark matter density profile by using the micro-lensing sky map, which can be used to further constrain various mechanisms of core formation.

To summarize, we apply the OGLE micro-lensing sky map to obtain by far the tightest constraint on the core size of the Milky Way dark matter halo. The core size value is 282^{+34}_{-31}pc and is independent of M_{lens} within a wide mass range. This result can potentially put stronger constraints on the cross-section of SIDM particles, the mass of ULDM/FDM. The core size can constrain the strength of the star formation process of the Milky Way. We acknowledge that we do not consider an off-center between the dark matter halo potential center and the Galactic center in our modeling which can be another interesting issue to probe. We also notice that the OGLE event rate sky map we use is only located at the Galactic center, and more data beyond the Galactic center region will greatly improve the constraint based on our model.

In the future, providing a wider range survey of micro-lensing event rate map (potentially Gaia archive data[44]), or novel statistical measures of micro-lensing event rate sky map, our method can be extended to a series of studies on the detailed structures of Milky Way dark matter halo.

Data and materials availability: The code supporting this work is available from the corresponding authors upon reasonable request.

The EMCEE package is available under MIT License in: https://emcee.readthedocs.io/en/stable/.

The Ultranest package is available in https://johannesbuchner.github.io/UltraNest/.

The OGLE catalogue is publicly available in: https://ogle.astrouw.edu.pl/.

———————

[*] all2b9s@mail.ustc.edu.cn
[†] wtluo@ustc.edu.cn
[‡] yifucai@ustc.edu.cn

[1] Planck Collaboration et al. Planck 2018 results. VI. Cosmological parameters. *Astronomy & Astrophysics*, 641:A6, September 2020.

[2] A. G. Riess et al. Snapshot distances to type ia supernovae: All in "one" night's work. *The Astrophysical Journal*, 504(2):935, sep 1998.

[3] S. Birrer et al. TDCOSMO. IV. Hierarchical time-delay cosmography - joint inference of the Hubble constant and galaxy density profiles. *Astronomy & Astrophysics*, 643:A165, November 2020.

[4] C. Hikage et al. Cosmology from cosmic shear power spectra with Subaru Hyper Suprime-Cam first-year data. *Publications of the Astronomical Society of Japan*, 71(2):43, April 2019.

[5] L. Verde et al. Tensions between the early and late Universe. *Nature Astronomy*, 3:891–895, September 2019.

[6] A. Leauthaud et al. Lensing is low: cosmology, galaxy formation or new physics? *Monthly Notices of the Royal Astronomical Society*, 467(3):3024–3047, feb 2017.

[7] B. Moore. Evidence against dissipation-less dark matter from observations of galaxy haloes. *Nature*, 370(6491):629–631, August 1994.

[8] J. F. Navarro et al. A Universal Density Profile from Hierarchical Clustering. *The Astrophysical Journal*, 490(2):493–508, December 1997.

[9] D. N. Spergel and P. J. Steinhardt. Observational Evidence for Self-Interacting Cold Dark Matter. *Physical Review Letters*, 84(17):3760–3763, April 2000.

[10] F. Jiang et al. A semi-analytic study of self-interacting dark-matter haloes with baryons. *arXiv e-prints*, pp. arXiv:2206.12425, June 2022.

[11] W. J. G. de Blok. The Core-Cusp Problem. *Advances in Astronomy*, 2010:789293, January 2010.

[12] A. Del Popolo and M. Le Delliou. Review of solutions to the Cusp-core problem of the ΛCDM Model. *arXiv e-prints*, pp. arXiv:2209.14151, September 2022.

[13] V. P. Debattista and J. A. Sellwood. Dynamical Friction and the Distribution of Dark Matter in Barred Galaxies. *The Astrophysical Journall*, 493(1):L5–L8, January 1998.

[14] J. Diemand et al. Clumps and streams in the local dark matter distribution. *Nature*, 454(7205):735–738, aug 2008.

[15] K. Bekki. Dark impact and galactic star formation: origin of the gould belt. *Monthly Notices of the Royal Astronomical Society: Letters*, 398(1):L36–L40, sep 2009.

[16] E. V. Karukes and P. Salucci. The universal rotation curve of dwarf disc galaxies. *PublicMonthly Notices of the Royal Astronomical Societyations of the*, 465(4):4703–4722, March 2017.

[17] T. K. Chan et al. The impact of baryonic physics on the structure of dark matter haloes: the view from the FIRE cosmological simulations. *Monthly Notices of the Royal Astronomical Society*, 454(3):2981–3001, December 2015.

[18] E. Tollet et al. NIHAO - IV: core creation and destruction in dark matter density profiles across cosmic time. *Monthly Notices of the Royal Astronomical Society*, 456(4):3542–3552, March 2016.

[19] I. D. Novikov et al. Primordial black holes. *Astronomy & Astrophysics*, 80(1):104–109, November 1979.

[20] B. Carr and F. Kühnel. Primordial Black Holes as Dark Matter: Recent Developments. *Annual Review of Nuclear and Particle Science*, 70:355–394, October 2020.

[21] M. Sasaki et al. Primordial black holes—perspectives in gravitational wave astronomy. *Classical and Quantum Gravity*, 35(6):063001, March 2018.

[22] J. Wang et al. Universal structure of dark matter haloes over a mass range of 20 orders of magnitude. *Nature*, 585(7823):39–42, September 2020.

[23] M. S. Delos and J. Silk. Ultradense dark matter haloes accompany primordial black holes. *Monthly Notices of the Royal Astronomical Society: Letters*, 520(3):4370–4375, April 2023.

[24] P. Mróz et al. Microlensing optical depth and event rate toward the galactic bulge from 8 yr of ogle-iv observations. *The Astrophysical Journal Supplement Series*, 244(2):29, oct 2019.

[25] P. Mróz et al. Microlensing Optical Depth and Event Rate in the OGLE-IV Galactic Plane Fields. *The Astrophysical Journals*, 249(1):16, July 2020.

[26] A. Wetzel et al. Public Data Release of the FIRE-2 Cosmological Zoom-in Simulations of Galaxy Formation. *The Astrophysical Journals*, 265(2):44, April 2023.

[27] H. Niikura et al. Constraints on earth-mass primordial black holes from OGLE 5-year microlensing events. *Physical Review D*, 99(8), apr 2019.

[28] A. Burkert. The structure of dark matter halos in dwarf galaxies. *The Astrophysical Journal*, 447(1), jul 1995.

[29] A. Klypin et al. ΛCDM-based models for the Milky Way and M31. I. Dynamical Models. *The Astrophysical Journal*, 573(2):597, jul 2002.

[30] P. Kroupa. On the variation of the initial mass function. *Monthly Notices of the Royal Astronomical Society*, 322(2):231–246, 04 2001.

[31] P. Mróz et al. No large population of unbound or wide-orbit jupiter-mass planets. *Nature*, 548(7666):183–186, jul 2017.

[32] A. Calamida et al. New insights on the galactic bulge initial mass function. *The Astrophysical Journal*, 810(1):8, aug 2015.

[33] D. Foreman-Mackey et al. emcee: The MCMC Hammer. *Publications of the Astronomical Society of the Pacific*, 125(925):306, March 2013.

[34] J. Buchner. A statistical test for Nested Sampling algorithms. *Statistics and Computing*, 26(1-2):383–392, January 2016.

[35] J. Buchner. Collaborative Nested Sampling: Big Data versus Complex Physical Models. *Publications of the Astronomical Society of the Pacific*, 131(1004):108005, October 2019.

[36] J. Buchner. UltraNest - a robust, general purpose Bayesian inference engine. *The Journal of Open Source Software*, 6(60):3001, April 2021.

[37] J. F. Navarro et al. The Structure of Cold Dark Matter Halos. *Astrophys. J.*, 462:563, May 1996.

[38] E. Kendall and R. Easther. The core-cusp problem revisited: ULDM vs. CDM. *Publications of the Astronomical*

Society of Australia, 37:e009, March 2020.

[39] A. Burkert. Fuzzy dark matter and dark matter halo cores. *The Astrophysical Journal*, 904(2):161, nov 2020.

[40] M. Rocha et al. Cosmological simulations with self-interacting dark matter – I. Constant-density cores and substructure. *Monthly Notices of the Royal Astronomical Society*, 430(1):81–104, 01 2013.

[41] J. G. de Swart et al. How dark matter came to matter. *Nature Astronomy*, 1:0059, March 2017.

[42] M. Rocha et al. Cosmological simulations with self-interacting dark matter – I. Constant-density cores and substructure. *Monthly Notices of the Royal Astronomical Society*, 430(1):81–104, 01 2013.

[43] A. Amruth et al. Einstein rings modulated by wave-like dark matter from anomalies in gravitationally lensed images. *Nature Astronomy*, 7:736–747, June 2023.

[44] Gaia Collaboration et al. Gaia Early Data Release 3. Summary of the contents and survey properties. *Astronomy & Astrophysics*, 649:A1, May 2021.